Influence of Crystal Structure on the Chemical Bonding Nature and Photocatalytic Activity of Hexagonal and Cubic Perovskite Compounds

Sun Hee Lee, In Young Kim, Tae Woo Kim, and Seong-Ju Hwang*

*Center for Intelligent Nano-Bio Materials (CINBM), Division of Nano Sciences and Department of Chemistry, Ewha Womans University, Seoul 120-750, Korea. *E-mail: hwangsju@ewha.ac.kr*
Received February 22, 2008

We have investigated the influence of the crystal structure on the chemical bonding nature and photocatalytic activity of cubic and hexagonal perovskite $A[Cr_{1/2}Ta_{1/2}]O_3$ (A = Sr, Ba) compounds. According to neutron diffraction and field emission-scanning electron microscopy, the crystal structure and particle size of these compounds are strongly dependent on the nature of A-site cations. Also, it was found that the face-shared octahedra in the hexagonal phase are exclusively occupied by chromium ions, suggesting the presence of metallic (Cr-Cr) bonds. X-ray absorption and diffuse UV-vis spectroscopic analyses clearly demonstrated that, in comparison with cubic $Sr[Cr_{1/2}Ta_{1/2}]O_3$ phase, hexagonal $Ba[Cr_{1/2}Ta_{1/2}]O_3$ phase shows a decrease of Cr oxidation state as well as remarkable changes in interband Cr *d-d* transitions, which can be interpreted as a result of metallic (Cr-Cr) interactions. According to the test of photocatalytic activity, the present semiconducting materials have a distinct activity against the photodegradation of 4-chlorophenol. Also the Sr-based compound was found to show a higher photocatalytic activity than the Ba-based one, which is attributable to its smaller particle size and its stronger absorption in visible light region.

Key Words : Hexagonal perovskite structure, Face sharing, Metal-metal bonds, Photocatalysis, Particle size

Introduction

Recently photocatalyst materials have attracted intense research activities since they can provide an economic and less-energy consuming option for purifying environment pollutions.[1,2] Among various semiconducting compounds, titanium oxide is of special importance as photocatalyst because of its many advantages such as low price, high stability, and non-toxicity.[2,3] However, its photocatalytic activity is severely limited by its large bandgap energy (E_g) of > 3.2 eV, which prevents it from harvesting photonic energy in visible and infrared region. In this regard, many attempts have been made to improve the photocatalytic activity of wide bandgap semiconductors through the control of band structure.[3-8] One of the most popular methods for the enhancement of photocatalytic activity is the chemical substitution of wide bandgap metal oxides like TiO_2. In particular, perovskite-structured ABO_3 metal oxides have been used as useful matrix for the chemical substitution, since they are very stable enough to form a solid solution with diverse metal ions. In this regard, there have been a great deal of studies on the cationic and anionic substitutions of perovskite-type metal oxides.[9-13] To dates, most of these researches have dealt with simple perovskite structure with cubic symmetry, in which BO_6 octahedra are linked by corner-sharing while larger A cations exist in dodecahedral sites. It has been well-known that the linkage patterns of BO_6 octahedra in the perovskite structure are strongly dependent on the nature of A-site cations.[14,15] In one instance, an increase of A-site cation radius gives rise to a structural modification into hexagonal perovskite structure having the face-sharing of BO_6 octahedra. In this hexagonal structure, the presence of significant metal-metal interactions between adjacent face-shared octahedra is expected to induce remarkable modifications in the band structure and physicochemical properties of the metal oxides. However, at the time of the present publication, we are aware of no systematic investigation on the effect of metal-metal interaction on the electronic structure and physicochemical property of perovskite-structured metal oxides.

In the present study, we have studied the influence of crystal structure on the band structure and chemical bonding nature of cubic and hexagonal structured $A[Cr_{1/2}Ta_{1/2}]O_3$ (A = Sr, Ba) compounds with various characterization tools including neutron diffraction (ND) and X-ray absorption spectroscopy (XAS). Also, their photocatalytic activity was systematically examined by monitoring the photodegradation of organic pollutants in the illuminated suspension of photocatalyst.

Experimental

According to the previous reports,[14,15] polycrystalline $A[Cr_{1/2}Ta_{1/2}]O_3$ (A = Sr, Ba) samples were prepared by conventional solid-state reaction with the stoichiometric mixture of $SrCO_3$, $BaCO_3$, Cr_2O_3, and Ta_2O_5 at 1350 °C under nitrogen flow. The crystal structures of the resulting compounds were studied by ND and powder X-ray diffraction (XRD, Cu Kα radiation) analyses. ND data of the two perovskite compounds were collected at room temperature over a 2θ range of 5°-160° using a step width of 0.05 using the high resolution powder diffractometer (HRPD, λ = 0.18352 nm) at the HANARO high-flux neutron reactor, beam port ST-2, in Korea Atomic Energy Research Institute

(KAERI). A thin-walled can of vanadium (height: 5 cm, diameter: 12 mm) was used to hold 8.5 g of the sample. The Rietveld refinement was carried out for the collected powder ND patterns using the FullProf program.[16] The morphologies of the $A[Cr_{1/2}Ta_{1/2}]O_3$ compounds were examined with field emission-scanning electron microscopy (FE-SEM, JEOL JSM-6700F). Diffuse reflectance UV-vis spectra were obtained on a Perkin-Elmer Lambda 35 spectrometer using $BaSO_4$ as a reference. The recorded reflectance data were converted to absorption data through the Kubelka-Munk function. XAS measurements were carried out at Cr K- and Ta L_{III}-edges with the extended X-ray absorption fine structure facility installed at the beam line 7C at the Pohang Light Source (PLS) in Korea. XAS data were collected at room temperature in a transmission mode using gas-ionization detectors. All the present spectra were calibrated carefully by measuring the spectrum of Cr or Ta metal. The photocatalytic degradation of 4-chlorophenol (4-CP) was tested in a Pyrex reactor (30 mL) with quartz window, which was subjected to radiation. Light from a 300-W Xe arc lamp (Oriel) passed through a 10-cm IR water filter and/or a UV cutoff filter ($\lambda > 300$ nm), then the filtered light was focused onto the reactor. The time-dependent changes of 4-CP concentration were spectrophotometrically monitored by measuring the absorbance at $\lambda = 225$ nm.

Results and Discussion

As presented in Figure 1, there are strong dependencies of the ND patterns of the $A[Cr_{1/2}Ta_{1/2}]O_3$ compounds on the type of A-site cations. The present ND pattern of the $Sr[Cr_{1/2}Ta_{1/2}]O_3$ phase could be well-reproduced with cubic perovskite structure (space group: *Fm-3m*), whereas that of the $Ba[Cr_{1/2}Ta_{1/2}]O_3$ phase could be well-fitted on the basis of six-layered perovskite-structure with hexagonal symmetry (space group: $P6_3/mmc$). This result is in good agreement with the previously reported powder XRD results.[14,15] The structural parameters of these phases obtained from Rietveld refinements are summarized in Table 1. As presented in Figure 2 and Table 1, there is a partial ordering of Cr and Ta ions in the octahedral sites of the cubic Sr-based compound. In the case of the hexagonal Ba-based phase, the octahedral sites of face-centered BO_6 octahedra are exclusively occupied by chromium ions whereas TaO_6 octahedra are linked by corner-sharing. According to the Rietveld refinements, the (Cr-Cr) bond in the hexagonal phase has a very short distance of 2.497 Å, strongly suggesting the presence of metallic (Cr-Cr) interactions. Such a presence of metallic bonds is expected to induce the shielding of Cr nuclear charge by delocalized electrons in (Cr-Cr) bonds. This expectation is supported by the longer distances of (Cr-

Table 1. Structural Parameters and Refinement Parameters Obtained from Rietveld Analysis for $A[Cr_{1/2}Ta_{1/2}]O_3$ (A = Sr, Ba)

Crystallographic parameters of $Sr[Cr_{0.5}Ta_{0.5}]O_3$ [a]						
atom	site	x	y	z	occupancy	B(Å^2)
Sr	8c	1/4	1/4	1/4	0.99(3)	1.04(2)
Cr(1)	4a	0	0	0	0.840(3)	0.39(3)
Cr(2)	4b	1/2	1/2	1/2	0.124(3)	0.39(3)
Ta(1)	4a	0	0	0	0.124(3)	0.39(3)
Ta(2)	4b	1/2	1/2	1/2	0.840(3)	0.39(3)
O	24e	0.2570(2)	0	0	0.99(3)	0.86(3)
Crystallographic parameters of $Ba[Cr_{0.5}Ta_{0.5}]O_3$ [b]						
atom	site	x	y	z	occupancy	B(Å^2)
Ba(1)	2a	0	0	0	1.0	0.9(1)
Ba(2)	2d	1/3	2/3	3/4	1.0	0.3(1)
Ba(3)	4f	1/3	2/3	0.1394(2)	1.0	0.62(6)
Cr	4e	0	0	0.1835(3)	1.0	0.3(1)
Ta	4f	1/3	2/3	0.5639(2)	1.0	0.64(6)
O(1)	6g	1/2	0	0	1.0	0.66(5)
O(2)	6h	0.148(8)	0.304(1)	1/4	1.0	1.01(9)
O(3)	12k	0.163(19)	0.340(0)	0.621(0)	1.0	0.77(6)

[a]Cubic, space group *Fm-3m* (no. 225), cell parameters: $a = b = c =$ 7.8832(2) Å, $\alpha = \beta = \gamma = 90^o$, χ^2: 9.18, R_{exp}: 3.85%, R_p: 9.35%, R_{wp}: 11.7%.; [b]Hexagonal, space group $P6_3/mmc$ (no. 194), cell parameters: $a = b =$ 5.7429(2) Å, $c =$ 18.7926(7) Å, $\alpha = \beta = 90^o$, $\gamma = 120^o$, χ^2: 11.4, R_{exp}: 3.01%, R_p: 9.25%, R_{wp}: 10.1%.

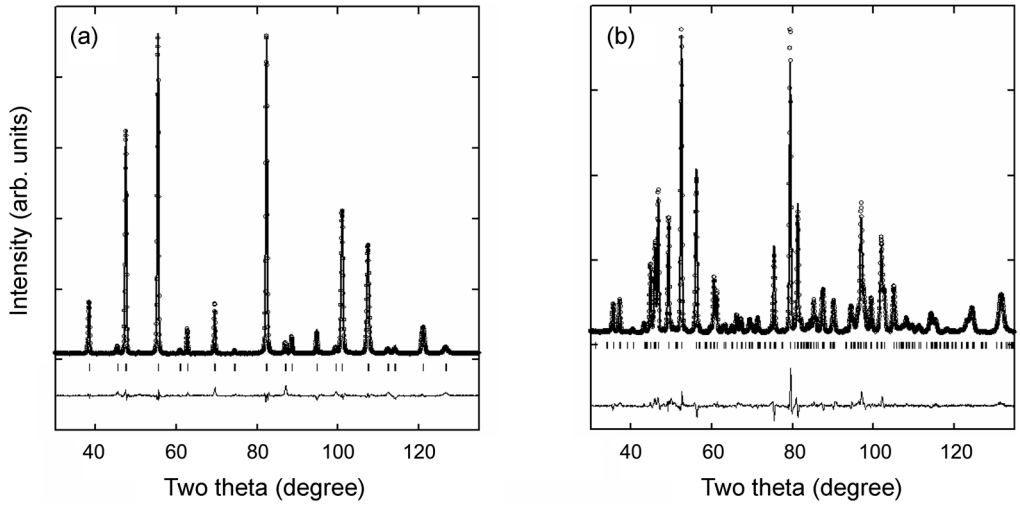

Figure 1. Experimental (circles) and fitted (solid lines) ND patterns of (a) $Sr[Cr_{1/2}Ta_{1/2}]O_3$ and (b) $Ba[Cr_{1/2}Ta_{1/2}]O_3$.

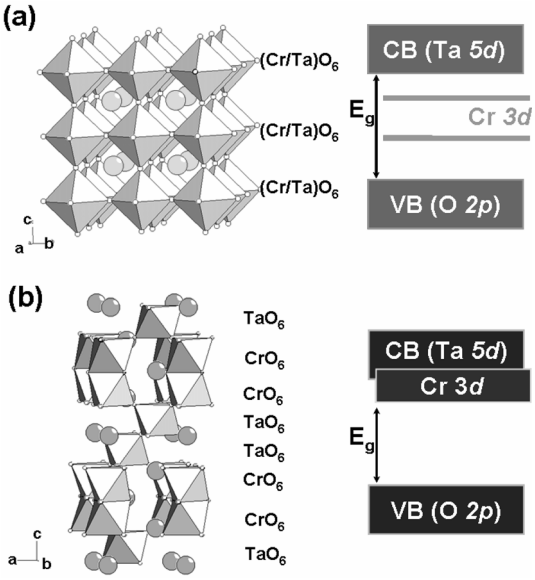

Figure 2. Schematic models for the crystal (left) and band (right) structures of (a) $Sr[Cr_{1/2}Ta_{1/2}]O_3$ and (b) $Ba[Cr_{1/2}Ta_{1/2}]O_3$.

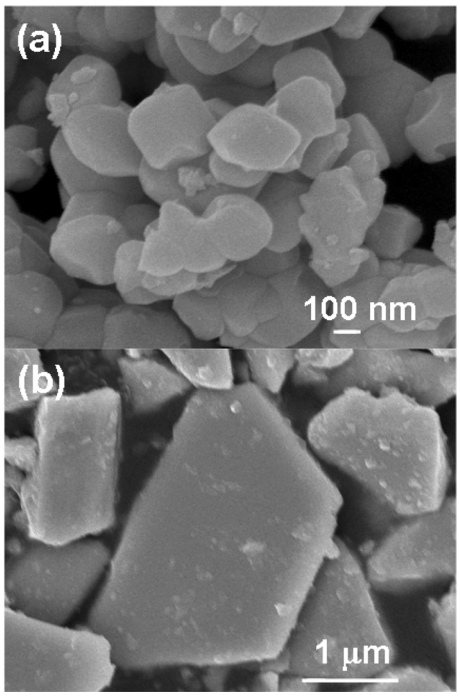

Figure 3. FE-SEM images of (a) $Sr(Cr_{1/2}Ta_{1/2})O_3$ and (b) $Ba(Cr_{1/2}Ta_{1/2})O_3$.

O) bonds in the hexagonal phase (1.960, 2.057, and 2.497 Å) than in the cubic one (1.9158 and 2.0276 Å).

We have examined the morphology of the $A[Cr_{1/2}Ta_{1/2}]O_3$ compounds using FE-SEM technique. As shown in Figure 3, both materials exhibit irregular polyhedral morphology with the particle size of ~100-300 nm for $Sr[Cr_{1/2}Ta_{1/2}]O_3$ and ~1-2 μm for $Ba[Cr_{1/2}Ta_{1/2}]O_3$. This observed smaller particles size of the Sr-based compound reflects its less efficient crystal growth.

The chemical bonding natures of the Cr and Ta ions have

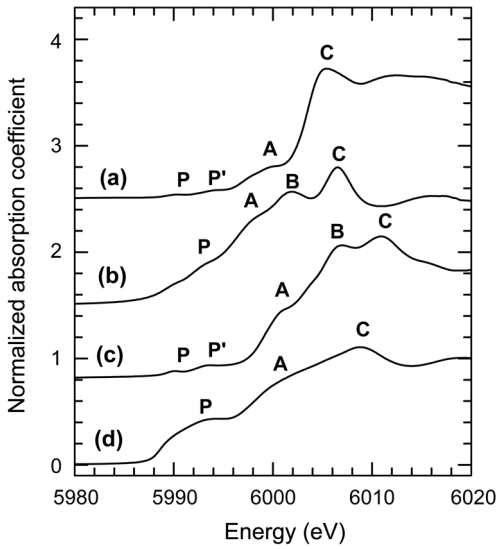

Figure 4. Cr K-edge XANES spectra for (a) $Sr[Cr_{1/2}Ta_{1/2}]O_3$, (b) $Ba[Cr_{1/2}Ta_{1/2}]O_3$, (c) Cr_2O_3, and (d) Cr metal.

been examined with X-ray absorption near-edge structure (XANES) spectroscopy at Cr K- and Ta L_{III}-edges. The Cr K-edge XANES spectra of $A[Cr_{1/2}Ta_{1/2}]O_3$ (A = Sr, Ba) are presented in Figure 4, together with those of Cr metal and Cr_2O_3. The $Sr[Cr_{1/2}Ta_{1/2}]O_3$ compound shows nearly identical edge energy to the reference $Cr_2^{III}O_3$, indicative of the trivalent oxidation state of chromium ions. On the contrary, the edge energy of the $Ba[Cr_{1/2}Ta_{1/2}]O_3$ is much lower than those of Cr_2O_3 and the Sr-based homologue, but closer to that of Cr metal, suggestive of lower Cr oxidation state than +3. This finding could be interpreted as strong evidence on the presence of metallic (Cr-Cr) bonds, leading to a partial shielding of the nuclear charge of Cr ions. This interpretation is in good agreement with the ND results showing longer (Cr-O) bond distances in the Ba-phase than in the Sr-phase. As plotted in Figure 4, all the present compounds exhibit pre-edge peaks P and P', and main-edge peaks A, B, and C, which correspond to the transitions from core 1*s* to unoccupied 3*d* or 4*p* levels, respectively.[6] In comparison with the cubic Sr-based compound, the hexagonal Ba-based homologue demonstrates low energy shifts of these features, confirming the presence of metallic (Cr-Cr) bonds.

The Ta L_{III}-edge XANES spectra of $A[Cr_{1/2}Ta_{1/2}]O_3$ (A = Sr, Ba) are plotted in Figure 5, together with those of Ta metal and Ta_2O_5. Regardless of the nature of A-site cation, the $A[Cr_{1/2}Ta_{1/2}]O_3$ compounds commonly exhibit nearly the same edge position as that of the $Ta_2^{V}O_5$, revealing the negligible dependence of Ta oxidation state on the crystal structure. This result coincides well with the present ND results showing the Ta ions are exclusively located in the octahedral sites of the corner-shared BO_6 octahedra, not in those of the face-shared octahedra. Hence, the electronic configuration of Ta ions is not modified by the metal-metal interaction occurring between face-centered octahedra. This conclusion is further supported by remarkable differences in edge energy between the spectra of $A[Cr_{1/2}Ta_{1/2}]O_3$ and Ta

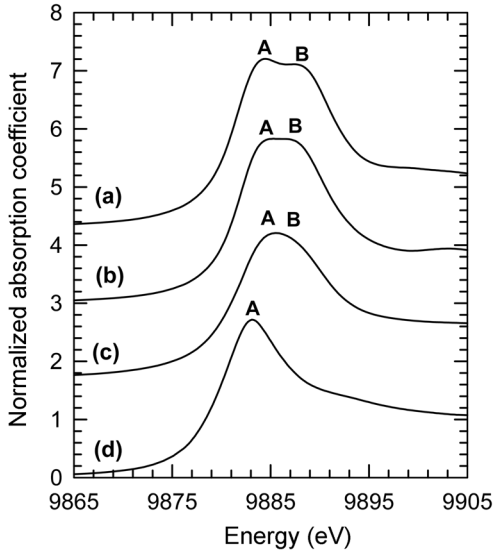

Figure 5. Ta L_{III}-edge XANES spectra for (a) $Sr[Cr_{1/2}Ta_{1/2}]O_3$, (b) $Ba[Cr_{1/2}Ta_{1/2}]O_3$, (c) Ta_2O_5, and (d) Ta metal.

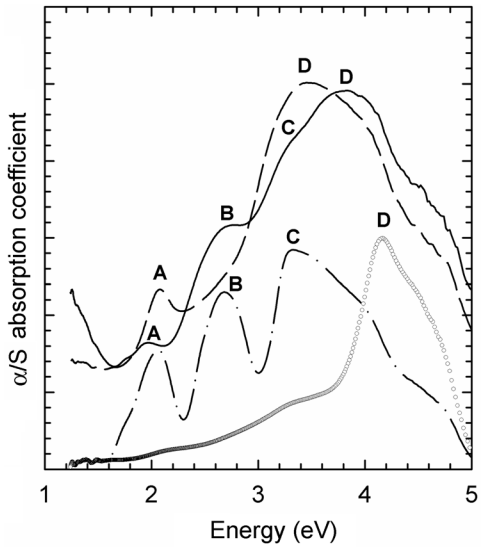

Figure 6. Diffuse reflectance UV-vis spectra for $Sr[Cr_{1/2}Ta_{1/2}]O_3$ (solid lines), $Ba[Cr_{1/2}Ta_{1/2}]O_3$ (dashed lines), Cr_2O_3 (dot-dashed lines), and Ta_2O_5 (circles).

metal. In Figure 5, all the present compounds show intense peaks A and B corresponding to $2s \rightarrow 5d_{t2g}$ and $2s \rightarrow 5d_{eg}$ transitions.[17] Since energy difference of these two peaks is proportional to the strength of crystal field around tantalum ions, a larger peak splitting in the Sr-based compound than in the Ba-based one highlights the greater crystal field strength in the former. This is in good agreement with the ND results revealing shorter (Ta-O) bond distances in the former (1.9158 and 2.0276 Å) than in the latter (1.951 and 2.0485 Å). The observed variation of crystal field strength could be understood as a result of unit cell contraction due to the smaller size of Sr^{2+} ion than Ba^{2+} ion.[18]

The diffuse reflectance UV-vis spectra of the $A[Cr_{1/2}Ta_{1/2}]O_3$ (A = Sr, Ba) compounds are plotted in Figure 6, together with those of Cr_2O_3 and Ta_2O_5. The $Sr[Cr_{1/2}Ta_{1/2}]O_3$ compound displays three characteristic absorption peaks A, B, C corresponding to Cr d-d interband transitions; $^4A_{2g} \rightarrow {}^4T_{2g}$, $^4T_{1g}$, and $^4T_{1g}$.[19] These features possess relatively similar energy and relative intensity for both $Sr[Cr_{1/2}Ta_{1/2}]O_3$ and Cr_2O_3, confirming the presence of Cr^{III} ions in the octahedral sites of the cubic perovskite structure. On the contrary, only one peak A is discernible for $Ba[Cr_{1/2}Ta_{1/2}]O_3$ in lower energy region of absorption edge, underscoring that the Cr 3d orbitals in this compound have quite different electronic configuration from that in the reference Cr_2O_3. This finding could be regarded as another support for the presence of metallic (Cr-Cr) interactions. Of noteworthy is that, in contrast to wide bandgap semiconductor Ta_2O_5, distinct absorptions in visible light region appear for both $A[Cr_{1/2}Ta_{1/2}]O_3$ materials, a result of band structure modification upon Cr incorporation. In comparison with the Ba-based compound, the Sr-based compound exhibits stronger absorptions in the visible light region, which is ascribable to the higher intensities of the interband peaks B and C. On the other hand, a closer inspection on the position of the peak D related to transition from valence band (VB) to conduction band (CB) reveals that the Ba-based phase possesses a slightly smaller E_g value than the Sr-based one, indicating the further decrease of E_g via the introduction of metallic (Cr-Cr) bonds. As plotted in the right panel of Figure 2, the formation of metallic (Cr-Cr) bonds in the hexagonal $Ba[Cr_{1/2}Ta_{1/2}]O_3$ phase increases the width of Cr 3d bands, leading to the effective overlap between Ta 5d and Cr 3d bands. Hence it gives rise to the disappearance of interband 3d states, which is in good agreement with the present UV-vis results revealing that the hexagonal Ba-based phase exhibits only one interband Cr 3d-related transition, in contrast to the reference Cr_2O_3 and the Sr-based phase.

We have investigated the photodegradation of 4-CP by the $A[Cr_{1/2}Ta_{1/2}]O_3$ (A = Sr, Ba) compounds to examine their photocatalytic activity. As plotted in Figure 7, the rate of 4-CP degradation under UV-vis irradiation (λ > 300 nm) is faster for the cubic Sr-based phase than for the hexagonal

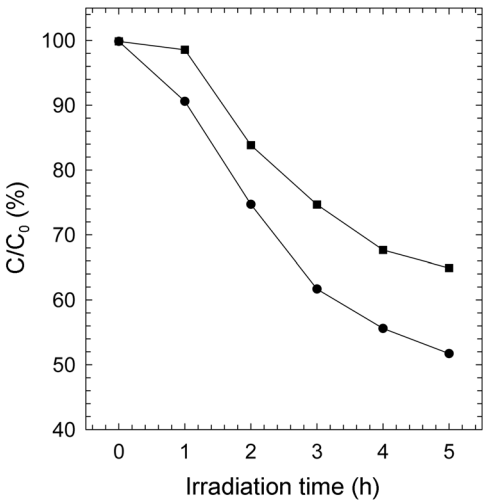

Figure 7. Variation of 4-CP concentration upon photoreaction (λ > 300 nm) for $Sr[Cr_{1/2}Ta_{1/2}]O_3$ (circles) and $Ba[Cr_{1/2}Ta_{1/2}]O_3$ (squares).

Ba-based one, indicating the higher activity of the former. This would be attributed to the smaller particle size of the cubic $Sr[Cr_{1/2}Ta_{1/2}]O_3$ compound than the hexagonal $Ba[Cr_{1/2}Ta_{1/2}]O_3$ compound, since a smaller particle size of the former implies its larger surface area, and such an increase of surface area provides this material with more reaction sites for photodegradation of organic molecules. As shown in Figure 6, the $Sr[Cr_{1/2}Ta_{1/2}]O_3$ compound displays more intense absorptions in the visible light region of ~2-3 eV, compared to the hexagonal $Ba[Cr_{1/2}Ta_{1/2}]O_3$ compound. Such variations of optical property also make a partial contribution to an enhancement of the photocatalytic activity of the Sr-based phase under UV-vis irradiation. On the other hand, we have also tested the photocatalytic activity of the $A[Cr_{1/2}Ta_{1/2}]O_3$ materials under visible light illumination (λ > 420 nm). But we only found the negligible visible light driven activity of the present materials, reflecting the fact that a decrease of E_g value upon Cr incorporation (*i.e.* the position of the peak D in Figure 6) is not large enough to create visible light harvesting ability.

Conclusion

The crystal structures, chemical bonding natures, and photocatalytic activities of cubic and hexagonal perovskite $A[Cr_{1/2}Ta_{1/2}]O_3$ (A = Sr, Ba) compounds have been systematically investigated. In comparison with cubic $Sr[Cr_{1/2}Ta_{1/2}]O_3$, hexagonal $Ba[Cr_{1/2}Ta_{1/2}]O_3$ phase with face-shared CrO_6 octahedra displays a lower Cr oxidation state and significant modifications in the number and energy of *d-d* transitions. This observation could be interpreted as a result of the metallic (Cr-Cr) interactions, which is further supported by the structural refinements based on the ND results. Also, it becomes certain that the present $A[Cr_{1/2}Ta_{1/2}]O_3$ semiconductors possess distinct photocatalytic activity against the photodegradation of 4-CP. Between these compounds, the Sr-based phase was found to show higher photocatalytic activity than the Ba-based one, which could be understood in terms of differences in their particle sizes and optical properties. Our current project is the incorporation of highly electronegative *p*-block elements into hexagonal perovskite structure, since this type of cation substitution has been known to be very effective in creating the visible light driven photocatalytic activity.[9-11]

Acknowledgments. This work was performed by the financial support of National R&D programs' of the Ministry of Science and Technology (MOST), Republic of Korea and supported partly by the SRC/ERC program of MOST/KOSEF (grant: R11-2005-008-00302-0). The experiments at PAL were supported in part by MOST and POSTECH. The authors thank to Prof. Seung-Joo Kim (Ajou University) for helping us to prepare the high temperature phase.

References and Notes

1. Honda, K.; Fujishima, A. *Nature* **1972**, *238*, 37.
2. Hoffmann, M. R.; Martin, S. T.; Choi, W.; Bahnemann, D. W. *Chem. Rev.* **1995**, *95*, 69.
3. Anpo, M. *Bull. Chem. Soc. Jpn.* **2004**, *77*, 1427.
4. Oh, W.-C.; Chen, M.-L. *Bull. Korean Chem. Soc.* **2008**, *29*, 159.
5. Asahi, R.; Morikawa, T.; Ohwaki, T.; Aoki, K.; Taga, Y. *Science* **2001**, *293*, 269.
6. Kim, T. W.; Hur, S. G.; Hwang, S.-J.; Park, H.; Choi, W.; Choy, J.-H. *Adv. Funct. Mater.* **2007**, *17*, 307.
7. Kim, T. W.; Hwang, S.-J.; Jhung, S. H.; Chang, J.-S.; Park, H.; Choi, W.; Choy, J.-H. *Adv. Mater.* **2008**, *20*, 539.
8. Kim, C.-S.; Jeong, H.-D. *Bull. Korean Chem. Soc.* **2007**, *28*, 2333.
9. Hur, S. G.; Kim, T. W.; Hwang, S.-J.; Park, H.; Choi, W.; Kim, S.-J.; Choy, J.-H. *J. Phys. Chem. B* **2005**, *109*, 15001.
10. Hur, S. G.; Kim, T. W.; Hwang, S.-J.; Choy, J.-H. *J. Photochem. Photobiol. A: Chem.* **2006**, *183*, 176.
11. Kim, T. W.; Hur, S. G.; Hwang, S.-J.; Park, H.; Park, Y;. Choi, W.; Choy, J.-H. *Mater. Res. Bull.* **2007**, *42*, 1914.
12. Yin, J.; Zou, Z.; Ye, J. *J. Phys. Chem. B* **2003**, *107*, 4936.
13. Hwang, D. W.; Kim, H. G.; Lee, J. S.; Kim, J.; Li, W.; Oh, S. H. *J. Phys. Chem. B* **2005**, *109*, 2093.
14. Hong, S. T.; Park, J. H.; Choy, J. H. *J. Phys. Chem.* **1995**, *99*, 6176.
15. Choy, J. H.; Park, J. H.; Hong, S. T.; Kim, D. K. *J. Solid State Chem.* **1994**, *111*, 370.
16. Rodriguez-Carvajal, J. *Physica B* **1993**, *192*, 55.
17. Kim, T. W.; Hur, S. G.; Han, A. R.; Hwang, S.-J.; Choy, J.-H. *J. Phys. Chem. C* **2008**, *112*, 3434.
18. Shannon, R. D. *Acta Cryst. A* **1976**, *32*, 751.
19. Huheey, J. H.; Keiter, E. A.; Keiter, R. L. *Inorganic Chemistry: Principles of Structure and Reactivity*; HarperCollins: New York, 1993.